

See discussions, stats, and author profiles for this publication at: <http://www.researchgate.net/publication/230588954>

Interdigitated array of Pt electrodes for electrical stimulation and engineering of aligned muscle tissue

ARTICLE *in* LAB ON A CHIP · JULY 2012

Impact Factor: 5.75 · DOI: 10.1039/c2lc40479f · Source: PubMed

CITATIONS

19

10 AUTHORS, INCLUDING:



Samad Ahadian

Tohoku University

49 PUBLICATIONS 285 CITATIONS

SEE PROFILE



Gulden Camci-Unal

Harvard University

40 PUBLICATIONS 538 CITATIONS

SEE PROFILE



Vahid Hosseini

ETH Zurich

21 PUBLICATIONS 129 CITATIONS

SEE PROFILE



Hirokazu Kaji

Tohoku University

87 PUBLICATIONS 1,318 CITATIONS

SEE PROFILE

Interdigitated array of Pt electrodes for electrical stimulation and engineering of aligned muscle tissue†

Samad Ahadian,^{‡a} Javier Ramón-Azcón,^{‡a} Serge Ostrovidov,^a Gulden Camci-Unal,^b Vahid Hosseini,^a Hirokazu Kaji,^c Kosuke Ino,^d Hitoshi Shiku,^d Ali Khademhosseini^{*abef} and Tomokazu Matsue^{*ad}

Received 1st May 2012, Accepted 22nd June 2012

DOI: 10.1039/c2lc40479f

Engineered skeletal muscle tissues could be useful for applications in tissue engineering, drug screening, and bio-robotics. It is well-known that skeletal muscle cells are able to differentiate under electrical stimulation (ES), with an increase in myosin production, along with the formation of myofibers and contractile proteins. In this study, we describe the use of an interdigitated array of electrodes as a novel platform to electrically stimulate engineered muscle tissues. The resulting muscle myofibers were analyzed and quantified in terms of their myotube characteristics and gene expression. The engineered muscle tissues stimulated through the interdigitated array of electrodes demonstrated superior performance and maturation compared to the corresponding tissues stimulated through a conventional setup (*i.e.*, through Pt wires in close proximity to the muscle tissue). In particular, the ES of muscle tissue (voltage 6 V, frequency 1 Hz and duration 10 ms for 1 day) through the interdigitated array of electrodes resulted in a higher degree of C2C12 myotube alignment (~80%) as compared to ES using Pt wires (~65%). In addition, higher amounts of C2C12 myotube coverage area, myotube length, muscle transcription factors and protein biomarkers were found for myotubes stimulated through the interdigitated array of electrodes compared to those stimulated using the Pt wires. Due to the wide array of potential applications of ES for two- and three-dimensional (2D and 3D) engineered tissues, the suggested platform could be employed for a variety of cell and tissue structures to more efficiently investigate their response to electrical fields.

Introduction

Skeletal muscle tissues have the capacity for limited self-repair; however, they lack the potential to restore damage caused by congenital defects, trauma, denervation and tumor ablation. In addition, intramuscular injection of myogenic cells, such as satellite cells or myoblasts, does not effectively induce tissue

repair due to low cell retention and survival, immunorejection and functional loss.¹ Since the ground-breaking work in the field of regenerative medicine by Vacanti and Langer,² many studies have been performed to generate engineered tissues and, consequently, to produce a reliable alternative for those in need of organ transplantation. Muscle tissue engineering has recently been suggested as a promising method to regenerate or recover damaged muscle tissue.^{3,4}

Engineered muscle tissue has *in vitro* applications, such as for drug screening^{5,6} or as bio-actuators.^{7,8} Drug screening using engineered muscle tissue can replace animal models and thereby reduce the considerable time and cost involved in animal experiments. Muscle tissues are also bio-actuators powered by the activation of actin-myosin molecular motors that convert chemical energy into mechanical force. Therefore, engineered muscle tissues are promising biomaterials for the construction of bio-actuators and for driving biodevices.⁸ Bio-actuators based on cardiomyocytes have already been developed.^{9,10} However, these devices use animals as the source of primary cardiomyocytes and offer little control over the contractile ability of cardiomyocytes.⁸ In this regard, skeletal muscle tissue is ideal for bio-actuators due to its controlled contraction. Moreover, skeletal muscle tissue may provide a more powerful force compared to the cardiac tissue.⁷

^aWPI-Advanced Institute for Materials Research, Tohoku University, Sendai, 980-8577, Japan.

E-mail: matsue@bioinfo.che.tohoku.ac.jp (T. Matsue); Fax: +81 22 795 6167

^bDepartment of Medicine, Center for Biomedical Engineering, Brigham and Women's Hospital, Harvard Medical School, Cambridge, Massachusetts 02139, USA and Harvard-MIT Division of Health Sciences and Technology, Massachusetts Institute of Technology, Cambridge, Massachusetts, 02139, USA

^cDepartment of Bioengineering and Robotics, Graduate School of Engineering, Tohoku University, Sendai, 980-8579, Japan

^dGraduate School of Environmental Studies, Tohoku University, Sendai, 980-8579, Japan

^eWyss Institute for Biologically Inspired Engineering, Harvard University, Boston, Massachusetts, 02115, USA

^fDepartment of Maxillofacial Biomedical Engineering and Institute of Oral Biology, School of Dentistry, Kyung Hee University, Seoul, 130-701, Republic of Korea.

E-mail: alik@rics.bwh.harvard.edu (A. Khademhosseini)

† Electronic supplementary information (ESI) available. See DOI: 10.1039/c2lc40479f

‡ These authors contributed equally to this work.

It is well known that muscle cells are able to differentiate under stimulation with an electrical field, which leads to an increase in myosin production and the formation of myofibers and contractile proteins.¹¹ In spite of significant progress in employing electrical fields for clinical purposes, the use of this tool to examine cell behavior and build functional tissues is in its infancy due to poor control over the underlying parameters.¹² Advances in microscale technologies used in biology and regenerative medicine¹³ can provide reliable methods and devices to enable the use of ES for tissue engineering applications in a precise and controllable manner. Interdigitated arrays of electrodes have been extensively employed for cell manipulation by the dielectrophoresis approach,^{14–16} however, the use of these devices for the ES of muscle tissue has not been reported. An interdigitated array of electrodes can create an electric field above and perpendicular to the electrode bands (Fig. 1). Here, we used an interdigitated array of electrodes for the ES of muscle tissue, which has the following advantages: (a) the electrodes are permanently positioned on the substrate and can therefore facilitate provide a highly reproducible and well-quantified electric field; (b) this technology makes it feasible to fabricate high resolution and complex electrode designs relevant to physiological feature sizes and architectures; (c) the ES is synchronized over the whole tissue; (d) lower energy is needed to create a

specified electric field compared to the conventional setups for ES. We should mention that traditional ES setups use a pair of conductive electrodes placed in close proximity to the muscle tissue. In such a configuration, the electric current should pass through the surrounding medium. Due to the inherent resistance of the medium, there is a decrease in the electric field, and the resulting diminished field may not lead to cell polarization and tissue stimulation.

In this study, we used a synthetic hydrogel, namely, gelatin methacrylate (GelMA),^{17,18} to fabricate 3D arrays of engineered muscle tissue. Hydrogels are hydrated networks of polymers that enable cell encapsulation.^{19,20} GelMA hydrogel is a photopolymerizable semi-natural hydrogel comprised of gelatin modified with methacrylic anhydride,²¹ and it is an attractive biomaterial for cell-based studies and tissue engineering applications.^{17,18}

During myogenesis, precursor cells commit to the myogenic lineage to form multinucleated muscle myofibers.²² The myogenic regulatory factors (MRFs) are major transcriptional regulators of myogenesis. The MRFs are a group of muscle specific transcription factors that include MyoD, Myf-5, myogenin and MRF4. MyoD and Myf-5 are expressed in growing, undifferentiated myoblasts and regulate myogenic determination.^{23,24} Myocyte-specific enhancer factor-2 (Mef2) proteins are a cohort of transcription factors that also play a

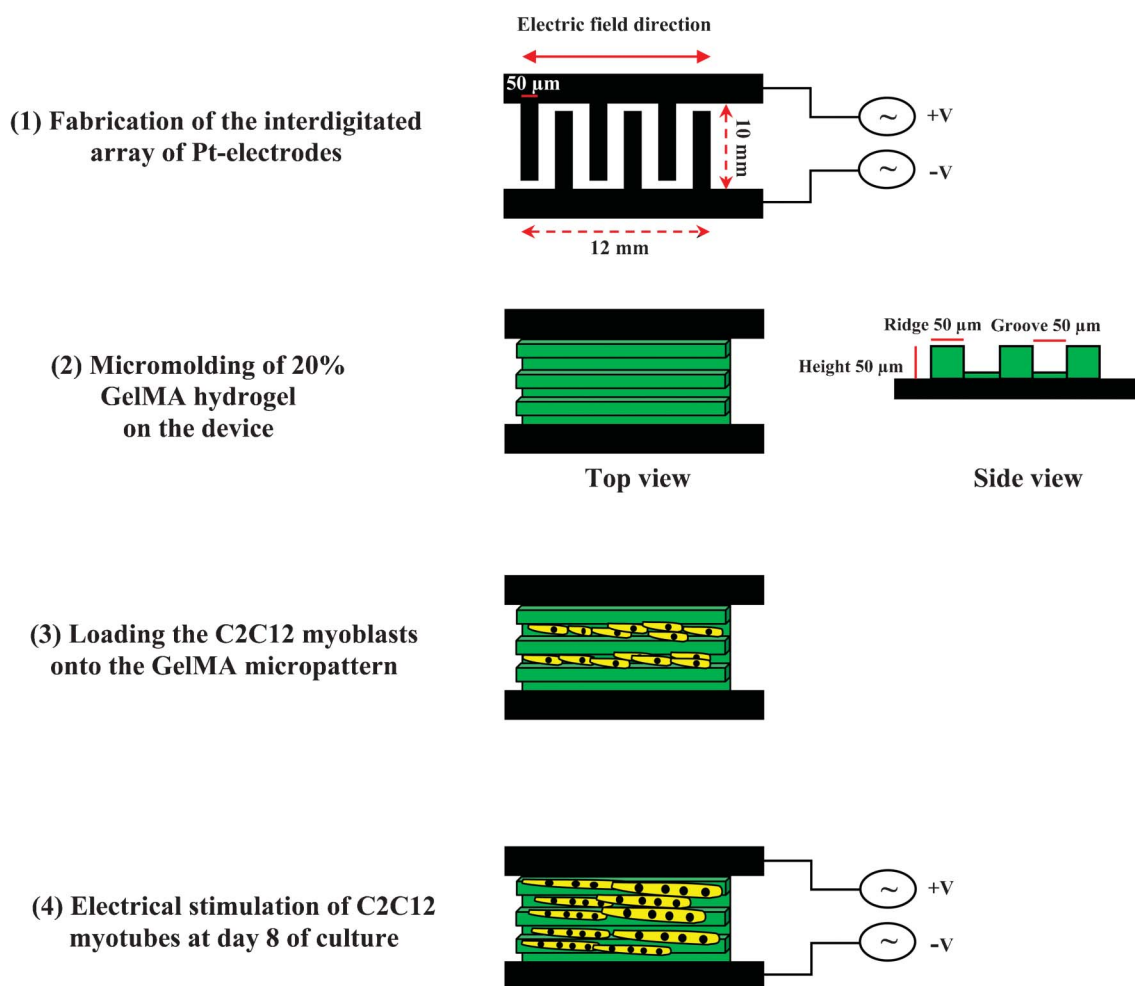


Fig. 1 Schematic of the experimental procedure used to obtain the functional muscle tissue.

crucial role in myoblast cell differentiation into muscle fibers. MyoD and Myf-5 expressions cause the activation of Mef2, which is essential to activate the transcription of myogenin and other muscle factors. Myogenin is only expressed upon muscle differentiation, and it can activate Mef2, ensuring a high level of differentiated skeletal muscle.²⁵ MRF4 and myogenin interact with muscle LIM protein (MLP) during muscle maturation and are highly expressed in mature adult skeletal muscle.²⁶ Here, we focused on the transcriptional analysis of MRFs (*i.e.*, MyoD, Myf-5, myogenin and MRF4), Mef2c and MLP to elucidate the maturation of the engineered muscle tissue. The expression of sarcomere contractile proteins [*i.e.*, sarcomeric actin, α -actinin, perinatal myosin heavy chain (MHC-pn), MHC-IIId/x, MHC-IIa and MHC-IIb] as markers of the differentiation of skeletal muscle tissue²⁷ was also investigated to evaluate the maturation of the fabricated muscle.

In this investigation, we fabricated a 3D functional muscle tissue using the microgrooved GelMA hydrogel as a scaffold. The constructed tissue was then subjected to ES as a means to accelerate the tissue maturation. An interdigitated array of Pt electrodes (IDA-Pt electrodes) was introduced as a platform for the ES of muscle tissue, and the resulting tissue was characterized and compared with that stimulated using the conventional ES setup used to mature muscle tissues *in vitro*. Due to variations in the application of ES to 2D and 3D engineered tissues,²⁸ the suggested platform could be employed to investigate the response of a variety of cell and tissue structures to DC and AC electrical fields in an efficient and precisely controlled manner.

Materials and methods

Chemicals

Positive g-line photoresist (*i.e.*, S1818) and developer (*i.e.*, MF CD-26) were obtained from Shipley Far East Ltd. (Tokyo, Japan). Hexamethyldisilazane was purchased from Tokyo Ohka Kogyo Co., Ltd. (Kanagawa, Japan). Methacrylic anhydride, 3-(trimethoxysilyl)propyl methacrylate (TMSPMA), gelatin Type A made of porcine skin and penicillin/streptomycin (P/S) were purchased from Sigma-Aldrich Chemical Co. (St. Louis, MO, US). 2-Hydroxy-1-(4-(hydroxyethoxy) phenyl)-2-methyl-1-propanone (*i.e.*, Irgacure 2959) was purchased from Ciba Chemicals (Osaka, Japan). Polydimethylsiloxane (PDMS) was purchased from Dow Corning Toray Co. Ltd. (Tokyo, Japan). Trichloro (1H, 1H, 2H, 2H-tridecafluoro-*n*-octyl) silane was purchased from Tokyo Chemical Industry Co. (Tokyo, Japan). Fetal bovine serum (FBS) was obtained from Bioserum, Japan. Dulbecco's modified Eagle's medium (DMEM), trypsin/EDTA, MEM essential amino acid, MEM nonessential amino acid and insulin were provided by Invitrogen, US.

GelMA hydrogel synthesis and preparation of its prepolymer

GelMA hydrogel was synthesized as described in our previous work.¹⁷ In summary, a high degree of methacrylation ($\sim 80\%$) was obtained by adding 8 mL methacrylic anhydride to 10 g of gelatin in Dulbecco's phosphate buffered saline (DPBS) for 3 h at 50 °C. The mixture was dialyzed with a 12–14 kDa cutoff dialysis membrane against distilled water for one week at 40 °C

and then lyophilized for one week. The GelMA hydrogel was kept at -20 °C until use.

GelMA hydrogel (20% w/v) was combined with the DPBS and 1% w/v photoinitiator (*i.e.*, Irgacure 2959), kept at 60 °C until fully dissolved, and then used for the experiments.

Cell culture

The C2C12 myoblast cell line was purchased from the American Type Culture Collection (ATCC), US. The cells were cultured in the DMEM supplemented with 10% FBS and 1% P/S, and they were used for the experiments at passage 7. The C2C12 myoblasts were trypsinized using 0.25% trypsin/0.1% EDTA when 70–80% confluence was reached. The cells were maintained in a cell culture incubator (Sanyo, Japan) with a 5% CO₂ atmosphere at 37 °C.

Micromolding of GelMA hydrogels and patterned culture of C2C12 myoblasts

At first, the PDMS stamp (see Supplementary information for the fabrication procedure of PDMS stamps†) was silanized using trichloro(1H, 1H, 2H, 2H-tridecafluoro-*n*-octyl) silane to prevent the adhesion of the GelMA polymer. IDA-Pt electrodes (see Supplementary information for detailed information on design and fabrication of electrodes†) were functionalized with the TMSPMA by coating the device with 2% TMSPMA in methanol for 1 h followed by 1 h drying at 80 °C. The GelMA hydrogel was then molded on the methacrylated IDA-Pt electrodes with the aid of the PDMS stamp such that the GelMA micropattern was perpendicular to the direction of the electrode bands as illustrated in Fig. 1. To do so, 20 μL of GelMA prepolymer was poured onto the Pt device. Then, the PDMS stamp was gently rubbed on the surface to completely fill the microgrooves of the stamp with the GelMA hydrogel, and the pattern was then exposed to 7 mW cm^{-2} UV light (Hayashi UL-410UV-1, Hayashi Electronic Shenzhen Co., Ltd., Japan) for 150 s. After that, the PDMS stamp was gently removed, leaving the GelMA micropattern on the IDA-Pt electrodes.

For cell culture on the GelMA micropattern, the C2C12 myoblasts were trypsinized, counted and resuspended in DMEM at a density of 1.5×10^6 cells mL^{-1} . Then, 100 μL of this suspension were pipetted onto the GelMA micropattern and incubated at 37 °C for 30 min to allow for cell seeding inside the micropattern grooves. Cells loaded within the GelMA micropattern were then cultured after adding sufficient culture medium. The procedure delineated here is shown schematically in Fig. 1. After 2 days of culture, the culture medium was replaced with the differentiation medium, which was DMEM with 2% horse serum, 1 nM insulin, and 1% P/S. During the culture period, the differentiation medium was replenished every 48 h.

Quantification of cellular alignment and elongation

After 1 day of culture, the C2C12 myoblasts were fixed with 3–4% paraformaldehyde for 12 min, followed by a wash with DPBS. The cells were treated with 0.3% Triton X-100 for 5 min at ambient temperature to make them permeable. Then the cells were exposed to 5% bovine serum albumin dissolved in DPBS for

15 min. The samples were stained with phalloidin (AlexaFluor® 594, Invitrogen, US) and 4,6-diamidino-2-phenylindole (DAPI) (Vector Laboratories Inc., Burlingame, CA, US), as recommended by the manufacturers, in order to reveal filamentous F-actin and cell nuclei, respectively. The stained pictures were recorded with a fluorescence microscope (Carl Zeiss Observer Z.1, Germany). The nuclear shape index (or circularity) and cell nuclear alignment were quantified as robust metrics for the average cell elongation and alignment, as previously documented.²⁹ The nuclear alignment angle was defined as the deviated angle of the major elliptical axis of individual nuclei from the micropatterned line and was measured using the NIH ImageJ software package (<http://rsbweb.nih.gov/ij/>). The alignment angles were then categorized in 10-degree increments, and all cells within less than 10 degrees were counted as aligned cells.³⁰ For the cells cultured on the unpatterned GelMA as the control sample, the alignment angle was considered to be the deviated angle from an arbitrary straight line crossing the sample. In addition, the nuclear shape index (circularity = $4 \times \pi \times \text{area} / \text{perimeter}^2$) of each individual cell nucleus was also quantified using the ImageJ software package. A shape index of 1 represents a non-elongated cell. At least 200 cell nuclei were considered to determine the cell alignment and circularity parameters, and all calculated values were checked manually to make sure that the results were accurate.

Myotube alignment and analysis

C2C12 muscle cells were fixed and permeabilized as described previously. A primary mouse monoclonal IgG antibody (ab-7784, Abcam®, Japan) to detect fast skeletal myosin was added to the underlying sample at a dilution of 1 : 1000 in DPBS and incubated at 4 °C for 24 h. The sample was then washed 3 times with DPBS and treated with secondary goat *anti*-mouse AlexaFluor® 488 antibody (Invitrogen, US) at a dilution of 1 : 1000 in DPBS and incubated at 37 °C for 1 h. Fluorescence microscopy images of the samples were taken for analysis of the stained myotubes, and at least 50 myotubes were considered for myotube quantification. The myotube length and alignment were quantified using the AxioVision Rel. 4.8 software package, and the myotube coverage area was computed with the NIH ImageJ software package.

Electrical stimulation of the engineered muscle tissue

On day 8 of culture, the engineered muscle tissue was electrically stimulated through the IDA-Pt electrodes as depicted in Fig. 1. As the control system, the muscle was stimulated with long platinum wires with 0.6 mm diameter placed 1.5 cm apart. For the ES of muscle tissue, the differentiation medium was replaced with the stimulation medium, which was composed of DMEM with 2% horse serum, 1 nM insulin, 2% MEM essential amino acid, 1% MEM nonessential amino acid and 1% P/S.³¹ Electrical pulses were applied to the muscle tissue using a waveform generator (WF 1946B Multifunction Synthesizer, NF Co., Japan) under two different ES regimes, namely, regime 1 (voltage 0.5 V, frequency 1 Hz, and duration 10 ms) and regime 2 (voltage 6 V, frequency 1 Hz, and duration 10 ms) for 3 days or 1 day, respectively. An oscilloscope (wave surfer 424; LeCroy Co., Japan) was used to confirm the generated electric current.

During ES of the muscle tissue, the stimulation medium was replenished every day to decrease the negative effects of collected charges in the medium.

RNA extraction and cDNA synthesis

Total RNA was extracted from 3 mg of the muscle tissue. The weighed tissue was placed in liquid nitrogen and thoroughly ground with a mortar and pestle. RNA was extracted using β -mercaptoethanol and purified according to the manufacturer's protocol (RNeasy®microkit, Qiagen, Venlo, Netherlands). Reverse transcription was performed according to the manufacturer's instructions (Quantitech Reverse Transcription, Qiagen, Venlo, Netherlands) for up to 3 μ g of total RNA. The temperature profile of the cDNA synthesis protocol was as follows: 12 μ l of sample (3 μ g of total RNA) was diluted with 14 μ l of RNase-free water and 4 μ l of gDNA wipeout buffer and incubated for 2 min at 42 °C and then cooled down to 4 °C. Quantiscript Reverse Transcriptase and Reverse Transcriptase primer mix were subsequently added, and the mixture was incubated for 15 min at 42 °C followed by incubation for 3 min at 95 °C. The samples were kept at 4 °C until use for the quantitative PCR (qPCR).

Real time PCR

Primer sets for GAPDH, MyoD, myogenin, MRF4, Myf-5, Mef2c, MLP, sarcomeric actin, α -actinin, MHC-pn, MHC-IId/x, MHC-IIa and MHC-IIb were obtained from Operon Biotechnologies (Tokyo, Japan) and validated for qPCR. The primer sequences are listed in the Supplementary data, Table S3.† Real time PCR was performed on a Roche Lightcycler 1.5 (Roche, Mannheim, Germany) using 2 μ l of cDNA, 2 μ l of the primer set (50 μ M) and 14 μ l of Lightcycler FastStart DNA Master SYBR Green 1 (Roche, Mannheim, Germany). Following an initial denaturation step at 95 °C for 10 min, real time PCR was performed over 45 cycles of 95 °C for 10 s, 62 °C for 10 s and 72 °C for 20 s, followed by a melt curve analysis. The expression of the target gene was assessed using the comparative method,³² and the results were normalized to the mouse GAPDH gene as the internal reference. Reported gene expression levels were the average of at least 2 independent experiments.

Statistical analysis

Statistically significant differences were revealed by the independent Student's *t* test for 2 groups of data using the MINITAB 16.0 statistical software package (Minitab Inc., State College, PA, US). All data are represented as average \pm standard deviation, and *p*-values less than 0.05 were deemed to be statistically significant.

Results and discussion

This work reports that IDA-Pt electrodes were more effective for the ES of muscle tissue than traditional setups with the following advantages: (a) because the electrodes were permanently fixed on the glass slide, they provided facile, highly reproducible and well-quantified electric fields; (b) it was feasible to fabricate high-resolution and complex electrode designs relevant to physiological

feature sizes and architectures; (c) the entire muscle tissue could simultaneously be stimulated; (d) a lower energy was needed to create a specified electric field as compared to conventional ES setups, therefore leading to less damage to the muscle tissue. Continuous ES could induce apoptosis and therefore decrease cell viability.³³ Indeed, some studies have reported more effective stimulation of the muscle tissue as compared to traditional ES setups (*i.e.*, through bringing the conductive electrodes in close proximity to the tissue). For instance, Ishibashi *et al.*³⁴ cultured C2C12 muscle cells on a porous alumina membrane masked by a hole-filled PDMS layer. A pair of electrodes were then placed at either side of the membrane. This device intensified the generated electric current at the hole in the PDMS layer. The results demonstrated that the voltage needed to stimulate the muscle tissue was over 10 times lower than the voltage required for the control. As indicated by the authors, only a few myotubes contracted using this configuration, probably because of the powerful adhesion of a single cell layer to the substrate.

Yamasaki *et al.* reported that after 8 days in differentiation medium, the C2C12 myotubes began to detach from the substrate so that the number of myotubes after 12 days of culture was less than that after 8 days of culture even though they were encapsulated in a 3D type-I collagen gel.⁸ Cooper *et al.* also observed myotube detachment from the substrate at days 5 and 6 after differentiation induction and suggested that this phenomenon resulted from high sarcomeric production and spontaneous contraction.³⁵ Massive detachment of myotubes from the Petri dish was also seen after around 8 days in the differentiation medium.³⁶ To address this problem, Nagamine *et al.*^{37,38} cultured myotube micropatterns and successfully transferred them onto the fibrin gel. Applying the electric field to the myotubes through the microelectrode arrays caused the contraction of myotubes within the fibrin gel without any defects. In another study from the same research group, the C2C12 myotubes were cultured on a microporous alumina membrane treated with a collagen layer on the upper side and a hole-filled PDMS layer on the underside. The stiffness of the collagen layer was close to the stiffness of the native muscle tissue (~ 12 kPa). Therefore, during ES, the myotubes started to contract without any problem.³¹ A method was also recently developed to transfer the aligned myotubes on the Petri dish to the type-I collagen gel.³⁹ These studies successfully solved the problem of adhesion of the muscle tissue sheets to the substrate; however, it is commonly known that the contraction of cells within fibrous extracellular matrices (ECMs) (*e.g.*, fibrin or type-I collagen gels) causes the detachment of these matrices from their environment and destroys the 3D architecture of the tissue.⁴⁰ In the current study, there was no difficulty in adhesion of the GelMA hydrogel to the substrate, probably due to the covalent bond between the methacrylate groups of the hydrogel and the acrylated substrate. As a result, the 3D cell-laden GelMA hydrogel fabricated here provided an appropriate milieu for the C2C12 muscle cells without considerable loss of the intended geometry over a prolonged time period. Cultivation of the engineered muscle tissue for a long time is crucial and permits the long-term investigation of muscle phenotype and function. As demonstrated by Engler and co-workers,⁴¹ functional muscle tissues preferentially occur on substrates with tissue-like

stiffnesses. In this regard, hydrogels are suitable substrates to provide stiffness and resemble the ECM for the muscle cells. However, the thickness and extensive swelling of hydrogels make it difficult to accomplish spatial patterning in a 3D environment.⁴² Here, we used micromolding to pattern the GelMA hydrogel in a facile and reproducible manner creating a 3D controlled micropattern for the C2C12 myoblasts. The 20% GelMA hydrogel employed here has a stiffness (~ 40 kPa) close to that of the native muscle tissue (~ 12 kPa).⁴³ The cells within the GelMA micropattern can proliferate and, in this regard, the GelMA micropattern has a great advantage over a broad range of synthetic polymers, providing topographical cues such as a rigid PDMS^{44,45} or poly(lactic-co-glycolic acid) fibers,⁴⁶ which do not allow the cells to grow or directly contact neighboring cells. Therefore, the micropatterned GelMA hydrogel exhibits superior performance over previous cell culture substrates for the construction of a functional muscle tissue.

Viability assessment of the C2C12 cells

High-energy ES has a negative effect on cell viability and, more importantly, on the performance of the engineered muscle tissue, leading to electrochemical damage of the tissue.⁴⁷ Such damage can be prevented by employing ES regimes with the minimum energy and by applying bipolar pulses. Voltage has been demonstrated to play a major role in the electrochemical damage of muscle tissue.⁴⁸ Therefore, the viability of the C2C12 cells was investigated by a live/dead assay. Fig. 2 presents stained pictures of electrically stimulated tissue (1 day under regime 2) and tissue that was not subjected to any electric field (for more details on the cell viability measurements, see the Supplementary information†). The staining revealed no statistically meaningful difference in cell viability between these tissues. The percentage cell viability for electrically stimulated tissue and non-stimulated tissue were $95.2 \pm 2.4\%$ and $96.6 \pm 2.2\%$, respectively.

Impedance spectroscopy analysis

Electrochemical impedance spectroscopy measurements are explained in the Supplementary information.† Fig. 3 (A) shows a schematic diagram of the Randles circuit between two neighboring electrode bands. The capacitance of the GelMA hydrogel layer on the IDA-Pt electrodes was in parallel with the capacitance of the electrode bands, which was constant and defined by the bands' geometrical characteristics. We assumed that impedance existed due to the diffusion of ions in solution. This phenomenon did occur but only influenced the impedance characteristics of the system at low frequencies. This effect was taken into consideration by adding the so-called Warburg impedance (W) to the lower branch of the equivalent circuit. The impedance response of the IDA-Pt electrodes may be mimicked by an electrically equivalent circuit⁴⁹ as presented in Fig. 3 (A). Capacitance of the IDA-Pt electrode ($C_{\text{IDA-Pt}}$) is the geometrical capacitance between two neighboring electrode bands in solution (see Supplementary information for the theoretical calculation of this parameter†), R_s is the solution resistance between two subsequent electrode bands, R_p represents the polarization resistance of the electrodes and, finally, W is the Warburg impedance, which is associated with the diffusion of elements in solution. The impedance of the system is given by

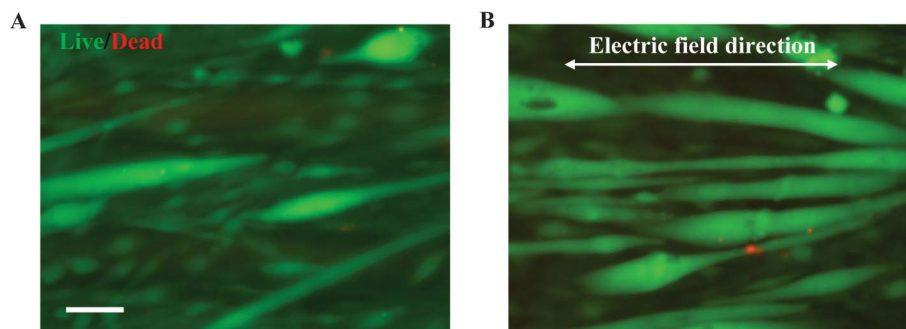


Fig. 2 Results of the live/dead assay for the engineered muscle tissue without ES (A) and with ES (B). The ES regime 2 (*i.e.*, voltage 6 V, frequency 1 Hz, and duration 10 ms) was applied at day 8 of culture for 1 day. No significant difference in the cell viability was observed between the samples (scale bar: 100 μm).

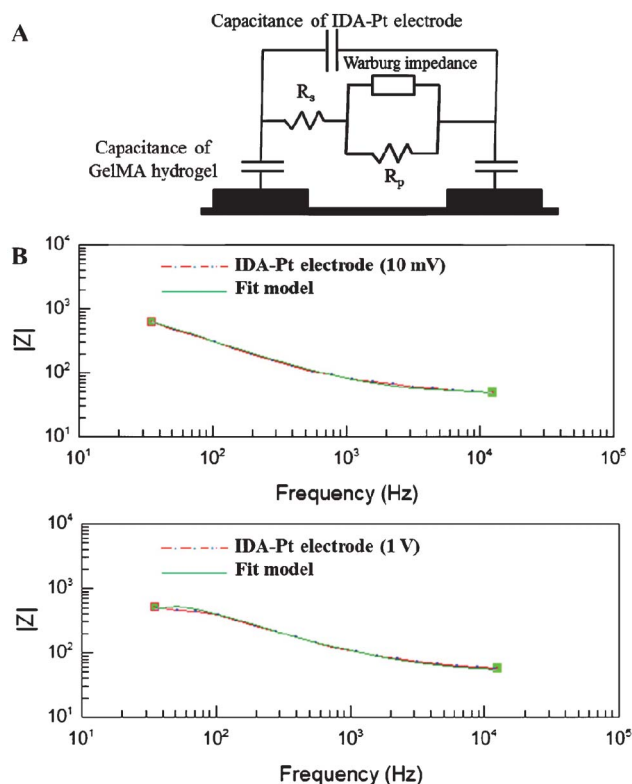


Fig. 3 Electrical characterization of the IDA-Pt electrodes. (A) Schematic representation of the electronic approximation of two neighboring electrode bands in the device. R_s and R_p represent the solution resistance between two bands and the polarization resistance of the electrodes, respectively. (B) Bode plots of the electrode impedance and fit model using the equivalent circuit for 10 mV and 1 V amplitudes.

$Z_{\text{IDA-Pt}} = 1/[(CPE)(j\omega)^\eta]$, where j is the imaginary unit and equals 1, ω is the angular frequency (rad s^{-1}), CPE is the capacitance of the double layer (F), and η is an empirical constant indicating the behavior of the CPE . When the exponent η is equal to 1, the CPE acts as a capacitor. If the value of η becomes 0, the CPE behaves as a resistor. The typical CPE value of η for platinum electrodes falls between 0.7 and 1.0.

The Bode plots of the IDA-Pt electrodes with input voltages of 10 mV and 1 V are presented in Fig. 3 (B). The obtained data were fit to the Randles circuit model, and the results are presented in

Table 1. Agreement between the measured data and the fitting spectra indicated that the equivalent circuit provided a reliable model to delineate the performance of the IDA-Pt electrodes. The R_p values (as a measure of corrosion resistance) were high, which is consistent with the stability of the Pt device. Due to high values of both R_p and η , we can approximate R_p as an open circuit and CPE as an ideal capacitor. Therefore, the impedance of the system could be simplified as a simple resistor-capacitor circuit that is dependent upon the frequency. Finally, making use of the approximation that most of the transmitted energy is at the fundamental frequency⁵⁰ (*e.g.*, for a 10 ms pulse, the energy is at 1/10 ms or 100 Hz), the sensed voltage was $\sim 10\%$ of the applied voltage. This result is reasonable because the GelMA hydrogel acts as an ideal isolated material with a conductivity of $\sim 0.08 \text{ mS cm}^{-1}$ as measured by the SG 3 conductimeter.

C2C12 myoblast alignment and elongation

The topography created by the GelMA hydrogel affected the cell morphology. Most C2C12 myoblast cells that were loaded onto the GelMA micropattern changed their morphology and oriented and elongated along the ridge-groove direction after 1 day of culture (Fig. 4). This phenomenon is referred to as *contact guidance*, in which most cells in the culture tend to orient and elongate in parallel (instead of perpendicular) to grooves or fiber axes.⁵¹ Focal adhesion proteins, such as vinculin and actin, orient themselves along the direction of the micropattern, a phenomenon that has been observed for many cell types.⁵² Note that the cells located on the ridge-groove boundaries demonstrated the highest degree of orientation and elongation as compared to other cells. This phenomenon was also observed in our previous work in which fibroblasts cultured within a 3D GelMA micropattern demonstrated a higher degree of alignment close to the edge surfaces of the micropattern compared to other parts of the structure.¹⁷

The degree of alignment for the C2C12 myoblasts within the GelMA micropattern was around 50% (Fig. 4). The GelMA micropattern was shown to be a suitable candidate for providing highly aligned muscle cells compared to the unpatterned GelMA hydrogel where the degree of alignment for the muscle cells was about 10% as reported in Fig. 4.

Another important factor by which to judge the cell growth is nuclear cell circularity. A decrease in the circularity of the cells over time implies a tendency to elongate and proliferate.^{53,54} As

Table 1 Main parameters calculated using the modified Randles equivalent circuit for IDA-Pt electrodes for the perturbation voltages 10 mV and 1 V

Perturbation voltage	R_s/Ω	R_p/Ω	$CPE/F\ s^{n-1}$	η	C_{IDA-Pt}^{a}/F
1 V	48.08 ± 1.58	$9.20E + 19 \pm 7.54E + 10$	$2.72E-05 \pm 2.43E-06$	0.80465 ± 0.011	$14.11E-12$
10 mV	45.80 ± 0.86	$1E + 20 \pm 4.20E + 10$	$2.75E-05 \pm 1.80E-06$	0.79606 ± 0.008	$14.11E-12$

^a Theoretically calculated (see Supplementary data†).

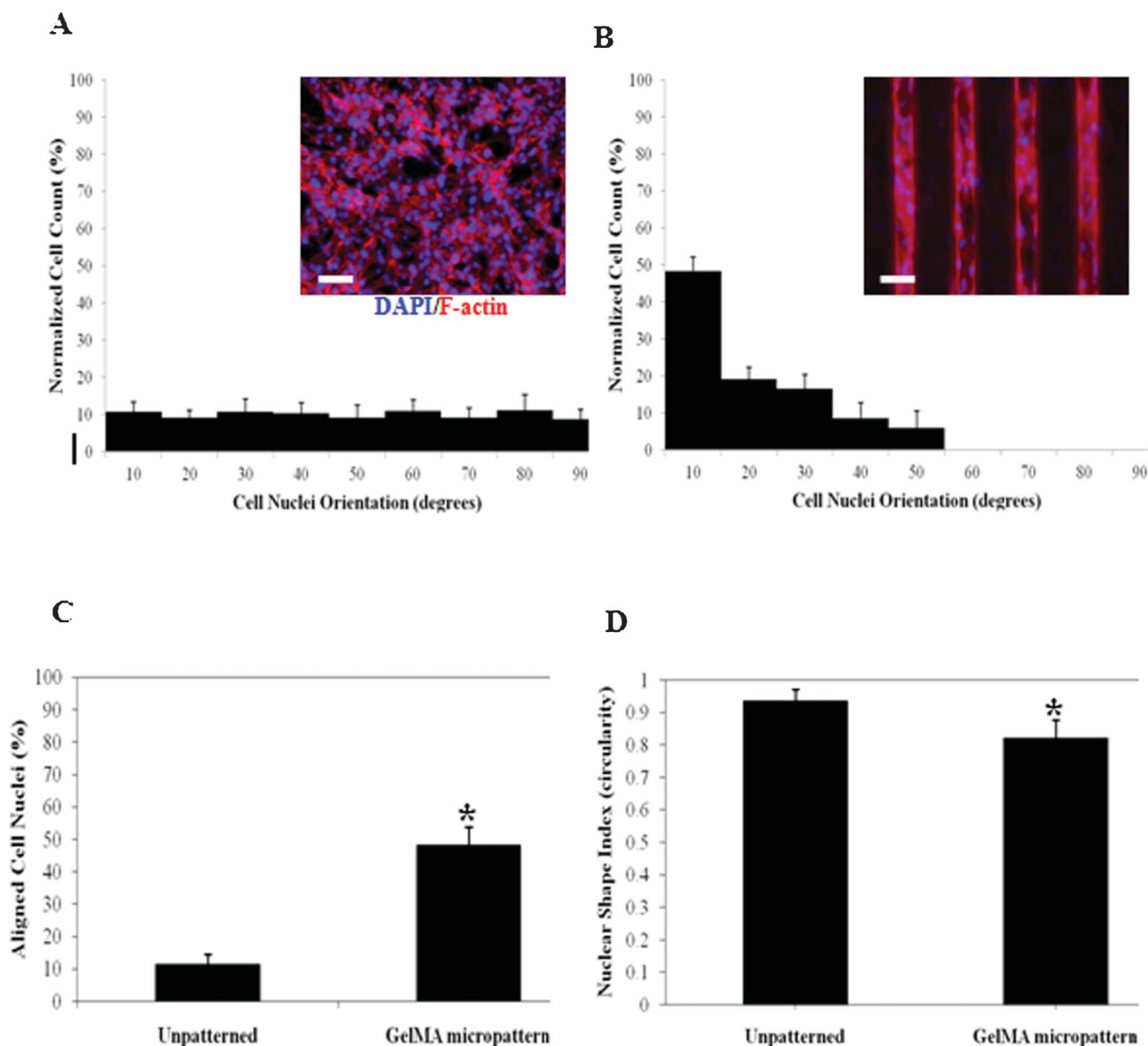


Fig. 4 C2C12 myoblast alignment and elongation on the GelMA micropattern and unpatterned GelMA hydrogel after 1 day of culture. Histograms of the relative cell nuclei alignment along the micropattern direction (or along an arbitrary straight line for the unpatterned control) in 10-degree increments showing a lower cellular alignment in the unpatterned control (A) compared to the GelMA micropattern (B). Representative photos of DAPI/F-actin staining of the samples are also presented in the corner of each histogram. (C) The mean percentage of aligned cell nuclei within 10 degrees of the preferred nuclear orientation demonstrating that C2C12 myoblasts in the GelMA micropattern were significantly more aligned than those in the unpatterned control. (D) The mean nuclear shape index (circularity) as a measure of cell elongation for the C2C12 myoblasts in the GelMA micropattern was significantly lower than that in the unpatterned control implying that the cells were more elongated within the GelMA micropattern (scale bar: 50 μm ; * $p < 0.01$).

indicated in Fig. 4, we found that the C2C12 myoblasts on the microgrooved GelMA hydrogel elongated significantly more than those on the unpatterned GelMA hydrogel ($p < 0.01$). Indeed, the amount of nuclear shape index is not varied much as

the cells align. This is because the value of 1 and 0 indicate the range from a circle to a line. Thus, typical values of cells do not approach 0. In addition, our results are within the range that has been observed by others for aligned cells.^{17,53}

C2C12 myotube alignment

A high degree of C2C12 myoblast alignment is needed to obtain highly aligned myotubes because the myoblasts fuse together to form myotubes in an end-to-end configuration.⁵⁵ Myotube alignment is crucial to maximize the contractility of muscle tissue.^{56,57} Construction of functional C2C12 myotubes in a 2D culture usually takes 2 weeks in the differentiation medium; however, cultivation of C2C12 muscle cells in a 3D environment promotes myotube formation. It has been reported that 8 days of culture in the differentiation medium is sufficient to induce myotube formation.¹¹ This conclusion is in agreement with our results, as C2C12 myotube formation was observed after 8 days of culture. As shown in Fig. 5 (A), C2C12 myotubes demonstrated a tendency to deviate from the GelMA micropattern

direction. This is an inherent property of C2C12 muscle cells when they are confined in a strip-like micropattern.⁵⁸ Applying ES led to a rearrangement of myotubes, resulting in their alignment along the direction of the electrical field (Fig. 5 (A)). Note that resulting myotubes after applying the ES under regime 2 became more mature with the observation of more striated myotubes (see Z-lines in Fig. 5 (A)). The rearrangement process of C2C12 myotubes was also observed in our previous work (see Movie 1⁵⁹). As shown in Fig. 5 (B), C2C12 myotubes exhibited a greater change in direction under ES regime 2 compared to regime 1 even when compared with conditions in which no electrical field was applied. Therefore, the degree of alignment for the myotubes under ES regime 1 was between that of the control and the aligned myotubes exposed to ES regime 2. Note

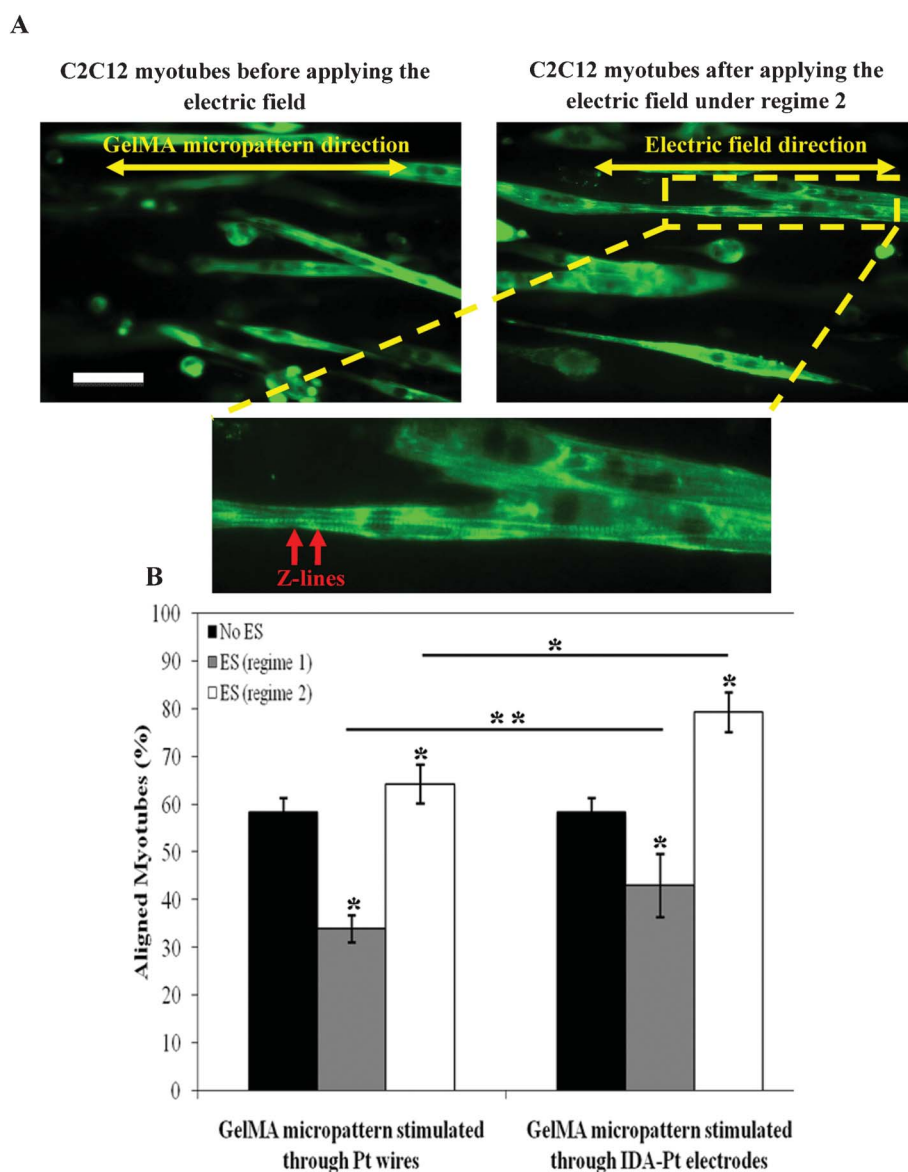


Fig. 5 C2C12 myotube alignment within the GelMA micropattern stimulated through IDA-Pt electrodes and using Pt wires under 2 ES regimes, namely, regime 1 (voltage 0.5 V, frequency 1 Hz, and duration 10 ms) and regime 2 (voltage 6 V, frequency 1 Hz, and duration 10 ms). (A) C2C12 myotubes as indicated by the myosin heavy chain (green) before and after ES under regime 2. Note that the myotubes were slanted towards the GelMA micropattern direction before applying the ES and Z-lines within striated myotubes were obvious after ES indicating highly mature myotubes. (B) The mean percentage of aligned myotubes within 10 degrees of the preferred myotube orientation (scale bar: 100 μm ; * $p < 0.001$ and ** $p < 0.05$).

that the myotube alignment for the unpatterned GelMA control was calculated to be around 10% as shown in the Supplementary information, Figure S1.† Interestingly, the ES of muscle tissue through the IDA-Pt electrodes had a significantly greater effect on the C2C12 myotube alignment than ES using Pt wires (Fig. 5 (B)). The contraction of engineered muscle tissue after 1 day of ES under regime 2 was also recorded and is provided in the Supplementary information, Movie S1.† As can be observed, the C2C12 myotubes contracted in the direction of the GelMA micropattern direction or the electrical field.

Dugan *et al.*⁶⁰ recently assessed the morphology and differentiation of C2C12 muscle cells on cellulose nanowhiskers. On these surfaces, the cell filopodia served as a robust measure to judge the cell area and its topography. Atomic force microscopy (AFM) analysis of myoblasts on the cellulose nanowhiskers revealed that most filopodia deviated from the preferred nanomaterial orientation. Furthermore, studies by Wan *et al.*^{58,61} also confirmed that C2C12 muscle cells tended to orient in a counter-clockwise direction when they were patterned in a stripe or circle-like

configuration. In our study, the C2C12 myoblasts were confined within a striped micropattern, and even though they were highly aligned and oriented along the groove direction, the myotubes demonstrated a highly aligned and slanted micropattern to the groove direction (Fig. 5). This parallel alignment of myotubes is a basic requirement of an engineered muscle tissue.⁶² Note that the close elasticity of the 20% GelMA hydrogel (~ 40 kPa) to that of the native muscle tissue (~ 12 kPa)⁴³ is an essential factor enabling such a myotube arrangement because the myotubes can move and alter their directions.

ES had a significant effect on the myotube alignment, changing the direction of the deviated myotubes in parallel to the direction of the applied electrical field. Tandon *et al.*⁶³ compared the effects of ES and topographical cues on cardiac cell alignment and elongation. They observed that applying an electrical field either parallel or orthogonal to the direction of the cells did not change the direction or elongation of the cells. Therefore, they concluded that the alignment and elongation pathway was saturated by the topographical cue and that the

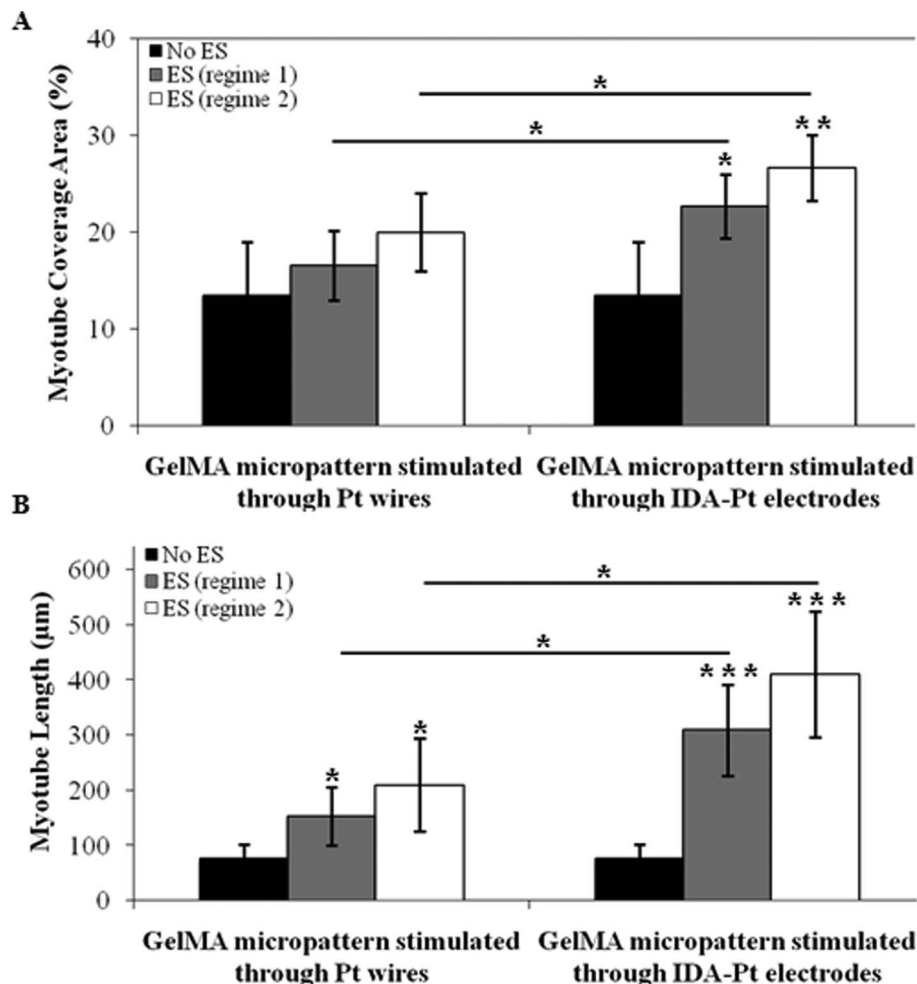


Fig. 6 Effect of ES on the myotube coverage area (A) and myotube length (B) of muscle fibers within the GelMA micropattern electrically stimulated with IDA-Pt electrodes or with Pt wires. ES was applied under 2 different regimes, namely, regime 1 (voltage 0.5 V, frequency 1 Hz, and duration 10 ms) and regime 2 (voltage 6 V, frequency 1 Hz, and duration 10 ms) at day 8 of culture. The myotube coverage area and myotube length in the GelMA micropattern stimulated by IDA-Pt electrodes were significantly increased compared with non-stimulated samples and those within the GelMA micropattern stimulated by Pt wires. Additionally, it seems that the ES under regime 2 is more effective than regime 1 ($*p < 0.05$, $**p < 0.01$ and $***p < 0.001$).

same signaling pathways control the cellular response to electrical and topographical cues. The same trend was reported by Au *et al.*^{64,65} in which cardiomyocytes were cultured on a chip to simultaneously evaluate the effects of electrical and topographical cues. However, it seems that the culture of cardiac cells on stiff materials, such as aluminum oxide, in these studies made it difficult for the cells to reorganize themselves and respond to the electrical field. As recently demonstrated by Bhana *et al.*,⁶⁶ cardiac cells cultured on substrates with a stiffness comparable to that of the native cardiac tissue exhibited optimal cell morphology and function.

C2C12 myotube morphology

Highly aligned myotubes stimulated through the IDA-Pt electrodes had more end-to-end myotube contacts as compared to those stimulated through the Pt wires because the muscle myofibers can move forward and backward more efficiently on the IDA-Pt electrodes. Therefore, a higher myotube coverage area was generally found on the GelMA micropattern stimulated through the IDA-Pt electrodes compared to those stimulated using the Pt wires (Fig. 6 (A)). Note that the ES of fabricated muscle tissue led to an increase in myotube formation for the muscle cells.

The average length of the myotubes within the GelMA micropattern stimulated through the IDA-Pt electrodes was significantly higher than that of the myotubes electrically stimulated by Pt wires, suggesting that the greater alignment of myotubes in the former case promoted the end-to-end connection of myotubes and therefore favored the assembly of myotubes (Fig. 6 (B)). This finding is in accordance with the work done by Huang *et al.*⁴⁵ where the myotubes were assembled on a nanofibrous, micropatterned and biocompatible polymer made of poly(L-lactide) and micropatterned PDMS. Note that ES under regime 2 led to a statistically meaningful increase in the myotube length in the GelMA micropatterns compared with the corresponding samples without any applied electrical field. However, this behavior was not observed for the myotubes stimulated under regime 1, indicating that 0.5 V is likely below the threshold voltage required for ES of a functional muscle tissue.⁶⁷

Change in the expression level of muscle maturation markers and sarcomere proteins due to the ES

Expression levels of target genes for muscle development were evaluated after applying the ES under regimes 1 and 2 (Fig. 7). The cultures that were electrically stimulated through the

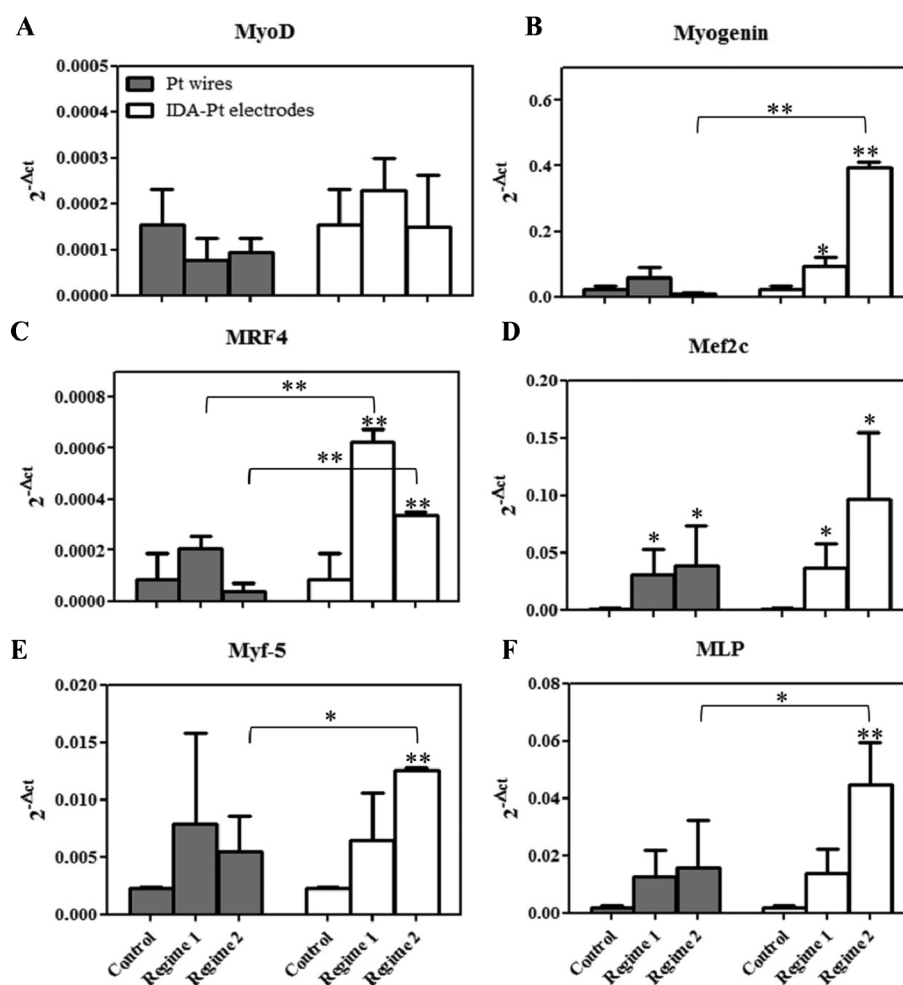


Fig. 7 Changes in the expression levels of MyoD (A), Myogenin (B), MRF4 (C), Mef2c (D), Myf-5 (E) and MLP (F) as a result of the different ES paradigms of regime 1 (voltage 0.5 V, frequency 1 Hz, and duration 10 ms), regime 2 (voltage 6 V, frequency 1 Hz, and duration 10 ms) and control (without ES). Expression levels were normalized with respect to the internal reference gene GAPDH (**p* < 0.05 and ***p* < 0.001).

IDA-Pt electrodes were compared to the corresponding samples stimulated by the Pt wires and those without ES (control samples). The genes under investigation were MRFs (*i.e.*, MyoD, myogenin, MRF4, and Myf-5), MLP and Mef2c.

Regarding the expression levels of the MRFs, MyoD expression significantly decreased over time and upon ES application (Fig. 7 (A)). However, the expression of myogenin was significantly higher for the muscle tissues stimulated through IDA-Pt electrodes under regime 2 than for those stimulated under regime 1, control samples and those stimulated by the Pt wires (Fig. 7 (B)). As shown in Fig. 7 (C), the same trend was observed in the expression level of MRF4, except that the muscle tissue stimulated through IDA-Pt electrodes under regime 1 showed the highest expression of this gene. Note that MRF4 expression was significantly higher for the fabricated muscle tissues stimulated through IDA-Pt electrodes under paradigm 2 compared to the corresponding control samples and those stimulated by the Pt wires. Even though the Mef2c expression levels were significantly higher for the electrically stimulated muscle tissues compared to the controls, there was no

statistically meaningful difference in the expression of this gene among the stimulated samples (Fig. 7 (D)). The Myf-5 gene was expressed at significantly higher levels for the samples stimulated using IDA-Pt electrodes under regime 2 compared to the control samples and those stimulated using Pt wires (Fig. 7 (E)). Finally, as demonstrated in Fig. 7 (F), MLP expression levels were higher for the cultures stimulated by the IDA-Pt electrodes under regime 2 compared with the controls and those stimulated through Pt wires.

Contraction of myotubes due to ES is associated with sarcomere development. As an electric field is applied, the sarcomere assembly is increased due to the manipulation of the intracellular Ca^{2+} transient through the depolarization of the cell membrane potential.³⁷ Note that ES under regime 2 evoked the contraction of myotubes as indicated in the Supplementary data, Movie S1.† In contrast, no such phenomenon was observed for the myotubes exposed to ES under regime 1. The expression levels of target genes for sarcomere protein development [*i.e.*, sarcomeric actin, α -actinin, perinatal myosin heavy chain (MHC-pn), MHC-IId/x, MHC-IIa and MHC-IIb] were evaluated due to the ES

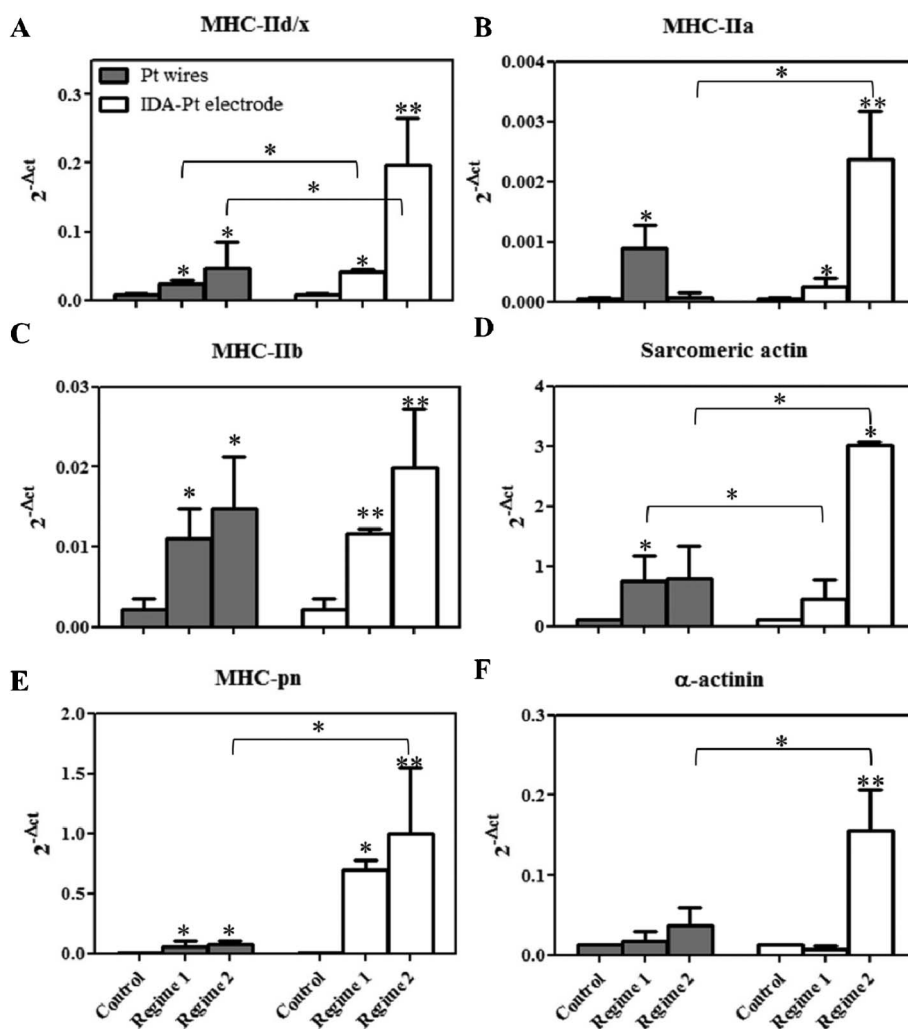


Fig. 8 Changes in the expression levels of MHC-IId/x (A), MHC-IIa (B), MHC-IIb (C), sarcomeric actin (D), MHC-pn (E) and α -actinin (F) as a result of the different ES paradigms of regime 1 (voltage 0.5 V, frequency 1 Hz, and duration 10 ms), regime 2 (voltage 6 V, frequency 1 Hz, and duration 10 ms) and control (without ES). Expression levels were normalized with respect to the internal reference gene GAPDH (* p < 0.05 and ** p < 0.001).

under regimes 1 and 2 as shown in Fig. 8. The cultures that were electrically stimulated using IDA-Pt electrodes were compared to their corresponding controls and those stimulated using the conventional ES setup of Pt wires.

As seen in Fig. 8, the expression levels of the underlying sarcomere contractile proteins markedly increased for the muscle tissues stimulated under regime 2 using IDA-Pt electrodes as compared with control samples and those stimulated with Pt wires. The most noticeable differences in gene expression levels between muscle tissues stimulated using IDA-Pt electrodes and the corresponding control samples were revealed in the expression levels of the sarcomere proteins α -actinin and actin (Fig. 8 (E) and (F)). Note that, except for MHC-IIId/x, there was no statistically significant difference in gene expression levels between the muscle tissues stimulated under paradigm 1 by IDA-Pt electrodes and Pt wires, implying that 0.5 V is likely below the threshold voltage required for the ES of a functional muscle tissue.⁶⁷

Taken together, we showed that different ES systems (or regimes) could alter the expression levels of muscle transcription factors and sarcomere contractile proteins and there is a direct relationship between the effectiveness of an ES system (or regime) and the expression levels of these genes. Also, we confirmed the potential of the muscle transcription factors and sarcomere contractile proteins as markers to monitor the maturation of fabricated muscle. Lassar *et al.*²⁵ remarked that myogenin and MRF4 were MRFs involved in the process of myotube maturation, and they are highly expressed in mature skeletal muscle. In contrast, MyoD and Myf-5 are expressed in proliferating myogenic cells, and their expression remains constant without significant changes over time. Therefore, they could not be used as muscle maturation markers. These conclusions are in agreement with our obtained results. The most significant changes were observed in the levels of MLP and sarcomere proteins. ES generally resulted in enhanced expression levels of these marker genes, indicating the development of more mature muscle tissue. As a result, it seems that the expression level of MLP and sarcomere components [*i.e.*, sarcomeric actin, α -actinin, perinatal myosin heavy chain (MHC-pn), MHC-IIId/x, MHC-IIa and MHC-IIb] are good potential indicators to evaluate muscle development at the transcriptional level.

Conclusions

Engineered skeletal muscle tissues are the subject of high interest because they are ideal candidates for regenerative medicine, drug screening and bio-actuator applications. In this study, we proposed the use of an interdigitated array of electrodes as a novel platform to electrically stimulate 3D engineered muscle tissue, which had the following advantages: (a) as the electrodes were permanently positioned on the substrate, they could facilitate provide a highly reproducible and well-quantified electric field; (b) it was feasible to fabricate high-resolution and complex electrode designs relevant to physiological feature sizes and architectures; (c) the ES was synchronized across the whole tissue; (d) lower energy was needed to create a specified electric field as compared to conventional ES setups. The engineered muscle tissues stimulated through the interdigitated array of electrodes demonstrated superior performance and maturation

compared to the corresponding tissues stimulated through the conventional setup (*i.e.*, through Pt wires in close proximity to the muscle tissue). Due to the wide potential applications of ES to 2D and 3D engineered tissues, the platform suggested here could be employed for a variety of cell and tissue structures to more efficiently investigate their responses to DC and AC electrical fields.

Acknowledgements

S.A. and J.R. designed the research and analyzed the results. S.A. and J.R. contributed equally to the work and wrote the paper. G.C.U. synthesized the GelMA hydrogel. S.A. and J.R. performed all other experiments. H.K., H.S., A.K., and T.M. supervised the research. All authors read the manuscript, commented on it, and approved its content. This work was supported by the World Premier International Research Center Initiative (WPI), MEXT, Japan.

References

- 1 C. A. Rossi, M. Pozzobon and P. De Coppi, *Organogenesis*, 2010, **6**, 167–172.
- 2 J. P. Vacanti, M. A. Morse, W. M. Saltzman, A. J. Domb, A. Perez-Atayde and R. Langer, *J. Pediatr. Surg.*, 1988, **23**, 3–9.
- 3 M. Koning, M. C. Harmsen, M. J. A. van Luyn and P. M. N. Werker, *J. Tissue Eng. Regen. Med.*, 2009, **3**, 407–415.
- 4 S. Hinds, W. Bian, R. G. Dennis and N. Bursac, *Biomaterials*, 2011, **32**, 3575–3583.
- 5 A. M. Ghaemmaghami, M. J. Hancock, H. Harrington, H. Kaji and A. Khademhosseini, *Drug Discovery Today*, 2012, **17**, 173–181.
- 6 H. Vandenburgh, *Tissue Eng., Part B: Rev.*, 2009, **16**, 55–64.
- 7 H. Fujita, T. Van Dau, K. Shimizu, R. Hatsuda, S. Sugiyama and E. Nagamori, *Biomed. Microdevices*, 2011, **13**, 123–129.
- 8 K. Yamasaki, H. Hayashi, K. Nishiyama, H. Kobayashi, S. Uto, H. Kondo, S. Hashimoto and T. Fujisato, *J. Artif. Organs*, 2009, **12**, 131–137.
- 9 M. Pilarek, P. Neubauer and U. Marx, *Sens. Actuators, B*, 2011, **156**, 517–526.
- 10 Y. Tanaka, Y. Yanagisawa and T. Kitamori, *Sens. Actuators, B*, 2011, **156**, 494–498.
- 11 H. Park, R. Bhalla and R. Saigal, *J. Tissue Eng. Regen. Med.*, 2008, **2**, 279–287.
- 12 E. Ghafar-Zadeh, J. R. Waldeisen and L. P. Lee, *Lab Chip*, 2011, **11**, 3031–3048.
- 13 A. Khademhosseini, R. Langer, J. Borenstein and J. P. Vacanti, *Proc. Natl. Acad. Sci. U. S. A.*, 2006, **103**, 2480–2487.
- 14 H. J. Lee, S. H. Lee, T. Yasukawa, J. Ramón-Azcón, F. Mizutani, K. Ino, H. Shiku and T. Matsue, *Talanta*, 2010, **81**, 657–663.
- 15 J. Ramón-Azcón, T. Yasukawa, H. J. Lee, T. Matsue, F. Sánchez-Baeza, M. –P. Marco and F. Mizutani, *Biosens. Bioelectron.*, 2010, **25**, 1928–1933.
- 16 J. Ramón-Azcón, S. Ahadian, R. Obregon, G. Camci-Unal, S. Ostrovidov, V. Hosseini, H. Kaji, K. Ino, H. Shiku, A. Khademhosseini and T. Matsue, *Lab Chip*, DOI: 10.1039/C2LC40213K.
- 17 H. Aubin, J. W. Nichol, C. B. Hutson, H. Bae, A. L. Sieminski, D. M. Crokek DM, P. Akhyari and A. Khademhosseini, *Biomaterials*, 2010, **31**, 6941–6951.
- 18 J. W. Nichol, S. T. Koshy, H. Bae, C. M. Hwang, S. Yamanlar and A. Khademhosseini, *Biomaterials*, 2010, **31**, 5536–5544.
- 19 N. A. Peppas, J. Z. Hilt, A. Khademhosseini and R. Langer, *Adv. Mater.*, 2006, **18**, 1345–1360.
- 20 B. V. Slaughter, S. S. Khurshid, O. Z. Fisher, A. Khademhosseini and N. A. Peppas, *Adv. Mater.*, 2009, **21**, 3307–3329.
- 21 A. I. Van Den Bulcke, B. Bogdanov, N. De Rooze, E. H. Schacht, M. Cornelissen and H. Berghmans, *Biomacromolecules*, 2000, **1**, 31–38.
- 22 M. Buckingham, L. Bajard, T. Chang, P. Daubas, J. Hadchouel, S. Meilhac, D. Montarras, D. Rocancourt and F. Relaix, *J. Anat.*, 2003, **202**, 59–68.
- 23 H. Arnold and T. Braun, *Int. J. Develop. Biol.*, 1996, **40**, 345–353.

- 24 K. I. Watt, R. Judson, P. Medlow, K. Reid, T. B. Kurth, J. G. Burniston, A. Ratkevicius, C. De Bari and H. Wackerhage, *Biochem. Biophys. Res. Commun.*, 2010, **393**, 619–624.
- 25 A. B. Lassar, S. X. Skapek and B. Novitch, *Curr. Opin. Cell Biol.*, 1994, **6**, 788–794.
- 26 S. Arber, G. Halder and P. Caroni, *Cell*, 1994, **79**, 221–231.
- 27 M. B. Taubman, C. W. Smith, S. Izumo, J. W. Grant, T. Endo, A. Andreadis and B. Nadal-Ginard, *J. Cell Biol.*, 1989, **108**, 1799–1806.
- 28 M. Hronik-Tupaj and D. L. Kaplan, *Tissue Eng., Part B: Rev.*, 2012, **18**, 167–180.
- 29 K. S. Brammer, S. Oh, C. J. Cobb, L. M. Bjursten, H. van der Heyde and S. Jin, *Acta Biomater.*, 2009, **5**, 3215–3223.
- 30 J. L. Charest, M. T. Eliason, A. J. Garcia and W. P. King, *Biomaterials*, 2006, **27**, 2487–2494.
- 31 H. Kaji, T. Ishibashi, K. Nagamine, M. Kanzaki and M. Nishizawa, *Biomaterials*, 2010, **31**, 6981–6986.
- 32 T. D. Schmittgen and K. J. Livak, *Nat. Protoc.*, 2008, **3**, 1101–1108.
- 33 M. H. Thelen, W. S. Simonides and C. van Hardeveld, *Biochem. J.*, 1997, **321**, 845–848.
- 34 T. Ishibashi, Y. Hoshino, H. Kaji, M. Kanzaki, M. Sato and M. Nishizawa, *Biomed. Microdevices*, 2009, **11**, 413–419.
- 35 S. T. Cooper, A. L. Maxwell, E. Kizana, M. Ghodussi, E. C. Hardeman, I. E. Alexander, D. G. Allen and K. N. North, *Cell Motil. Cytoskeleton*, 2004, **58**, 200–211.
- 36 P. Bajaj, B. Reddy, L. Millet, C. Wei, P. Zorlutuna, G. Bao and R. Bashir, *Integr. Biol.*, 2011, **3**, 897–909.
- 37 K. Nagamine, T. Kawashima, T. Ishibashi, H. Kaji, M. Kanzaki and M. Nishizawa, *Biotechnol. Bioeng.*, 2010, **105**, 1161–1167.
- 38 K. Nagamine, T. Kawashima, S. Sekine, Y. Ido, M. Kanzaki and M. Nishizawa, *Lab Chip*, 2011, **11**, 513–517.
- 39 N. F. Huang, R. J. Lee and S. Li, *Am. J. Transl. Res.*, 2010, **2**, 43–55.
- 40 B. M. Gillette, J. A. Jensen, B. Tang, G. J. Yang, A. Bazargan-Lari, M. Zhong and S. K. Sia, *Nat. Mater.*, 2008, **7**, 636–640.
- 41 A. J. Engler, M. A. Griffin, S. Sen, C. G. Bönnemann, H. L. Sweeney and D. E. Discher, *J. Cell Biol.*, 2004, **166**, 877–887.
- 42 S. Khetan and J. A. Burdick, *Soft Matter*, 2011, **7**, 830–838.
- 43 P. M. Gilbert, K. L. Havenstrite, K. E. G. Magnusson, A. Sacco, N. A. Leonardi, P. Kraft, N. K. Nguyen, S. Thrun, M. P. Lutolf and H. M. Blau, *Science*, 2010, **329**, 1078–1081.
- 44 W. Bian and N. Bursac, *Biomaterials*, 2009, **30**, 1401–1412.
- 45 N. F. Huang, S. Patel, R. G. Thakar, J. Wu, B. S. Hsiao, B. Chu, R. J. Lee and S. Li, *Nano Lett.*, 2006, **6**, 537–542.
- 46 K. J. Aviss, J. E. Gough and S. Downes, *Eur. Cells Mater.*, 2010, **19**, 193–204.
- 47 T. Y. Kostrominova, D. E. Dow, R. G. Dennis, R. A. Miller and J. A. Faulkner, *Physiol. Genomics*, 2005, **22**, 227–243.
- 48 K. Donnelly, A. Khodabukus, A. Philp, L. Deldicque, R. G. Dennis and K. Baar, *Tissue Eng., Part C*, 2009, **16**, 711–718.
- 49 D. Berdat, A. C. Martin Rodriguez, F. Herrera and M. A. M. Gijs, *Lab Chip*, 2008, **8**, 302–308.
- 50 N. Tandon, A. Marsano, R. Maidhof, K. Numata, C. Montouri-Sorrentino, C. Cannizzaro, J. Voldman and G. Vunjak-Novakovic, *Lab Chip*, 2010, **10**, 692–700.
- 51 S. A. Riboldi, M. Sampaolesi, P. Neuenschwander, G. Cossu and S. Mantero, *Biomaterials*, 2005, **26**, 4606–4615.
- 52 C. M. Hwang, Y. Park, J. Y. Park, K. Lee, K. Sun, A. Khademhosseini and S. H. Lee, *Biomed. Microdevices*, 2009, **11**, 739–746.
- 53 R. G. Thakar, M. G. Chown, A. Patel, L. Peng, S. Kumar and T. A. Desai, *Small*, 2008, **4**, 1416–1424.
- 54 M. Versaevel, T. Grevesse and S. Gabriele, *Nat. Commun.*, 2012, **3**, 671.
- 55 P. Clark, G. A. Dunn, A. Knibbs and M. Peckham, *Int. J. Biochem. Cell Biol.*, 2002, **34**, 816–825.
- 56 W. Bian, M. Juhas, T. W. Pfeiler and N. Bursac, *Tissue Eng. A*, 2012, **18**, 957–967.
- 57 R. L. Lieber and J. Fridén, *Muscle Nerve*, 2000, **23**, 1647–1666.
- 58 L. Q. Wan, K. Ronaldson, M. Park, G. Taylor, Y. Zhang, J. M. Gimble and G. Vunjak-Novakovic, *Proc. Natl. Acad. Sci. U. S. A.*, 2011, **108**, 12295–12300.
- 59 V. Hosseini, S. Ahadian, S. Ostrovidov, G. Camci-Unal, S. Chen, H. Kaji, M. Ramalingam and A. Khademhosseini, *Tissue Eng. Part A*, In press.
- 60 J. M. Dugan, J. E. Gough and S. J. Eichhorn, *Biomacromolecules*, 2010, **11**, 2498–2504.
- 61 L. Q. Wan and G. Vunjak-Novakovic, *Commun. Integr. Biol.*, 2011, **4**, 745–748.
- 62 H. Liao and G.-O. Zhou, *Tissue Eng., Part B: Rev.*, 2009, **15**, 319–331.
- 63 N. Tandon, C. Cannizzaro, P.-H. G. Chao, R. Maidhof, A. Marsano, H. T. H. Au, M. Radisic and G. Vunjak-Novakovic, *Nat. Protoc.*, 2009, **4**, 155–173.
- 64 H. T. H. Au, I. Cheng, M. F. Chowdhury and M. Radisic, *Biomaterials*, 2007, **28**, 4277–4293.
- 65 H. T. H. Au, B. Cui, Z. E. Chu, T. Veres and M. Radisic, *Lab Chip*, 2009, **9**, 564–575.
- 66 B. Bhana, R. K. Iyer, W. L. K. Chen, R. Zhao, K. L. Sider, M. Likhitanichkul, C. A. Simmons and M. Radisic, *Biotechnol. Bioeng.*, 2010, **105**, 1148–1160.
- 67 A. Khodabukus and K. Baar, *Tissue Eng., Part C*, 2012, **18**, 349–357.